

Experimental investigation on air-jet loom sub-nozzles for weft yarn insertion

*Original*

Experimental investigation on air-jet loom sub-nozzles for weft yarn insertion / Belforte, Guido; Mattiazzo, Giuliana; Testore, Francantonio; Visconte, Carmen. - In: TEXTILE RESEARCH JOURNAL. - ISSN 0040-5175. - STAMPA. - 81:8(2011), pp. 791-797. [10.1177/0040517510391694]

*Availability:*

This version is available at: 11583/2420935 since: 2017-01-24T14:23:21Z

*Publisher:*

SAGE

*Published*

DOI:10.1177/0040517510391694

*Terms of use:*

This article is made available under terms and conditions as specified in the corresponding bibliographic description in the repository

*Publisher copyright*

(Article begins on next page)

# **Experimental investigation on air-jet loom sub-nozzles for weft yarn insertion**

G. Belforte, G. Mattiazzo, F. Testore, C. Visconte

*Politecnico di Torino, Department of Mechanical and Aerospace Engineering*

*Corso Duca degli Abruzzi, 24*

*10129 TORINO, Italy*

Tel: +39 011 090 6925, Fax: +39 011 090 6999, e-mail: [carmen.visconte@polito.it](mailto:carmen.visconte@polito.it)

**Authors' version (final draft post-refereeing)**

**Published in:**

***Textile Research Journal* , 81 (8) (2014), 791-797**

**DOI: 10.1177/0040517510391694**

Keywords: air-jet loom, sub-nozzles, weft passage.

## **Abstract**

The analysis of the airflow from sub-nozzles having different emitting cross-section is described. At first, tests were carried out outside the profiled reed and comparison between nozzles was made in terms of air velocity distribution, jet spreading, consumption and exerted drag force. Subsequently, in order to analyse the interaction between the jet emitted by a sub-nozzle and the loom profiled reed, some velocity measurements were repeated inside the weft passage, at various distances from the nozzle exit. Finally, a high-speed camera was used to visualize the weft yarn crossing the weft passage.

## **1. Introduction**

The air guiding system used in air-jet weaving includes a profiled reed equipped with multiple nozzles. Air flow issuing from the main nozzle drags the yarn by friction forces, increasing its kinetic energy; since the main jet is scattered at a certain distance from the main nozzle, sub-nozzles are provided along the profiled reed to support the yarn during its crossing. Even though many improvements have been made to this system [1], the large consumption of air is probably the

main drawback of this kind of loom. Therefore, many research works have been addressed to improve the performance of main and sub-nozzles for energy saving, as reported, for example, by Ishida and Okajima [2] and by Göktepe and Bozkan [3]. A few authors reported that the airflow in the weft passage resulted from the interaction of the sub-nozzles jet with the profiled reed. Shintani and Okajima [4], for example, measured the airflow velocity distribution inside a profiled reed under different leakage conditions through the front and the back of the profile reed.

The experimental investigation described here deals with the analysis of the airflow from sub-nozzles that have different emitting cross-sections, both considering the free jet and the jet interacting with the profiled reed. A new criterion for efficiency evaluation, measurement of the drag force exerted by the sub-nozzle airflow on the weft yarn, was introduced with respect to previous studies [5]. This measurement also gave a criterion for the optimization of the positioning of the sub-nozzles on the loom. At first, tests were carried out outside the profiled reed; the behaviour of the nozzles was compared in terms of velocity distribution, jet spreading, consumption and drag force exerted on the weft yarn. Subsequently, in order to analyse the interaction between the jet emitted by a sub-nozzle and the loom profiled reed, some velocity measurements were repeated inside the weft passage, at various distances from the nozzle exit. The motion of the weft yarn inside the weft passage was also observed by means of a high-speed camera. This analysis allowed clear identification of the drag mechanism and gave useful advice for the system set-up.

## **2. Experimental details: characterization of nozzles airflow**

Three commercial sub-nozzles, whose geometry dimensions are summarized in Table 1, were analysed.

Nozzles A and B, produced by the same manufacturer, differ because of the exit section; in fact, nozzle A is a porous nozzle, while nozzle B is a single hole nozzle. Nozzle D, produced by another manufacturer, has the same emitting cross-section of nozzle B, but is characterized by a feeding duct with a different geometry.

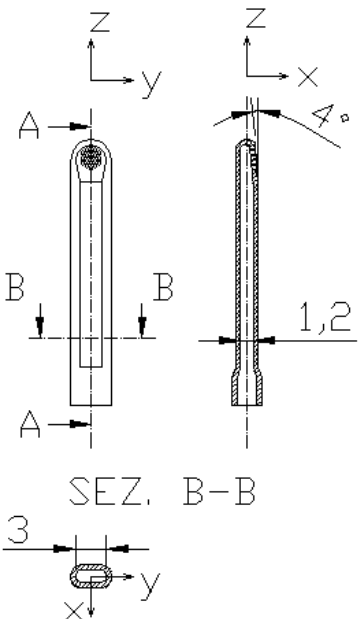
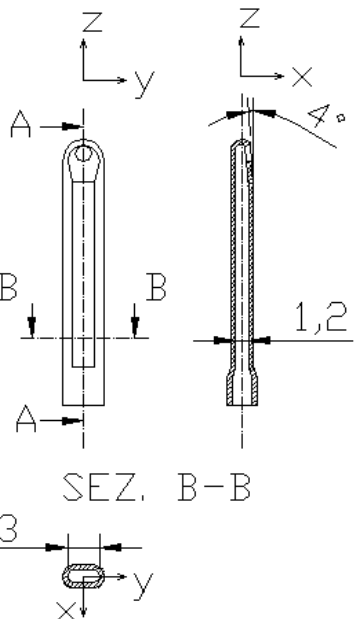
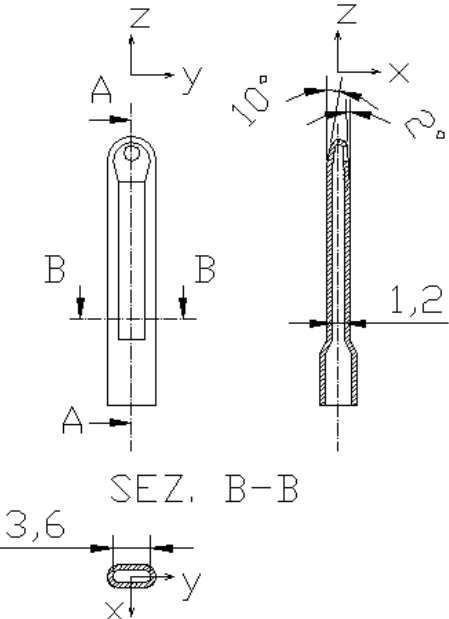
		
<b>Nozzle A</b> <b>Porous</b>	<b>Nozzle B</b> <b>Single hole –</b> <b>Small internal duct</b>	<b>Nozzle D</b> <b>Single hole -</b> <b>Large internal duct</b>
<b>N. of holes = 19</b>	<b>N. of holes = 1</b>	<b>N. of holes = 1</b>
<b>Holes diameter</b> <b>= 0.35 mm</b>	<b>Hole diameter</b> <b>= 1.5 mm</b>	<b>Hole diameter</b> <b>= 1.5 mm</b>
<b>Total area</b> <b>= 1.83 mm<sup>2</sup></b>	<b>Total area</b> <b>= 1.76 mm<sup>2</sup></b>	<b>Total area</b> <b>= 1.76 mm<sup>2</sup></b>

Table 1 Geometry dimensions of the sub-nozzles under test.

Initially, the consumption of the nozzles was evaluated. Figure 1 shows the measuring set-up, assembled according to the standard ISO 6358 [6]. It includes: a source (1); a filter (2); a pressure regulator (3), to set the supply pressure of the component under test; an on-off valve (4); a variable-area flow-meter (5) (Rota Yokogawa; measurable flow rates: 14-136 l/min ANR; accuracy  $\pm 2.5\%$  of full scale); a pipe (6) ( $d_3 = 6$  mm) for temperature measurement, equipped with a thermometer T; a pipe (7) ( $d_1 = 2$  mm) for measurement of supply pressure  $P_u$ , equipped with a pressure transducer (ENTRAN; full scale = 15 bar; sensitivity = 0.58 mV/bar); and the component under test, that is the sub- nozzle, freely discharging into the surroundings.

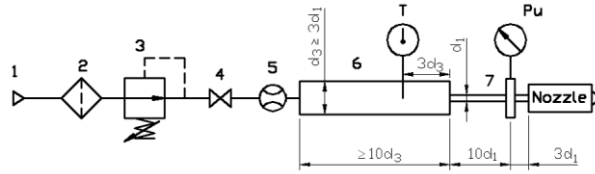


Figure 1 Measuring set-up for evaluation of nozzles' consumption.

Having measured ambient temperature  $T_0$  and ambient pressure  $P_0$  with a thermometer and a barometer respectively, the nozzle supply pressure  $P_u$  was initially set at 0.5 bar; flow rate  $Q$  and flow temperature  $T$  were measured. Subsequently, the nozzle supply pressure was increased and the previously described procedure was repeated. A supply pressure range of 0,5÷6 bar was analysed. Figure 2 shows flow rate consumption versus supply pressure for all the nozzles in the study. The pneumatic conductance of each nozzle, reported in Table 2, was worked out from these data. According to the standard ISO 6358, the values shown are referred to ANR, that is ambient temperature  $T_0 = 293$  K and ambient pressure  $P_0 = 1$  bar [6].

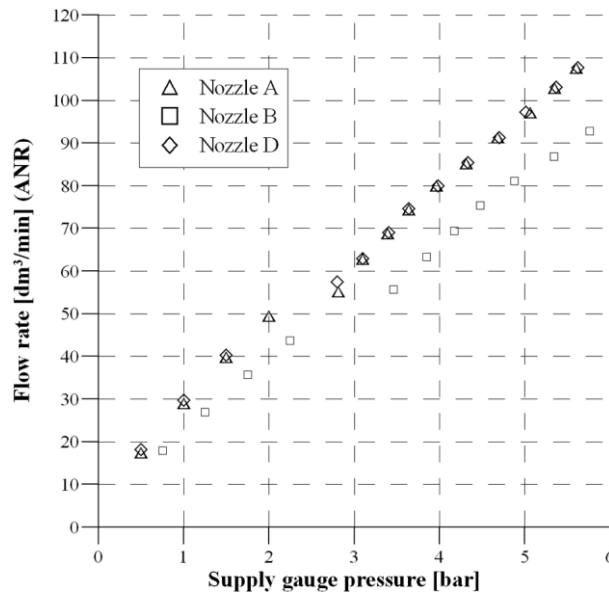


Figure 2 Nozzles' consumption.

Pneumatic conductance C [dm <sup>3</sup> /(min*bar)] (ANR)		
Nozzle A	Nozzle B	Nozzle D
16.13	13.65	16.12

Table 2 Pneumatic conductance of the tested nozzles.

As shown, even if an increase of outflow resistance could be expected in a porous nozzle, nozzle A had a conductance higher than that of nozzle B, thanks to its higher total exit section. Comparing the behaviour of nozzle B and nozzle D, the influence of the internal feeding duct on nozzle conductance can be noted. In fact, even if the emitting cross-section of these nozzles is the same in terms of shape and area, nozzle D exhibited a higher pneumatic conductance thanks to its more efficient internal design. Its feeding duct, in fact, has a larger cross-section and is provided by a sort of guiding elbow at its tip, conveying the flow towards the exit section. Subsequently, jet velocity profiles were obtained at distances  $x$  equal to 40, 74 and 90 mm from the nozzle exit.

A stainless steel Prandtl type Pitot probe (diameter = 0.5 mm), connected to a U-shaped water column manometer, was used to measure air jet stagnation pressure. The Pitot tube was mounted, with the head parallel to the flow direction and the stem perpendicular to it, on a precision manual linear positioner (NEWPORT; sensitivity = 1  $\mu$ m), allowing displacements along two perpendicular directions on an axial cross-section of the jet.

Initially, the probe was placed at a distance  $x = 40$  mm from the nozzle exit; using the precision manual positioner, the probe was displaced with a step of 2 mm to scan the jet axial section.

The stagnation pressure reading for each position was recorded. The nozzle supply was finally cut off. The data reduction equation for the determination of velocity  $v$  is:

$$v = \sqrt{\frac{2}{\rho} \cdot p_s} ,$$

where  $p_s$  is the stagnation pressure reading from the Pitot tube and  $\rho$  is the air density. The air density was determined from the ideal gas relationship:

$$\rho = \frac{P_0}{R \cdot T_0}$$

where  $P_0$  is the ambient pressure,  $R$  is the gas constant for air and  $T_0$  is the absolute ambient temperature. The air density was determined once by measuring the ambient temperature and pressure with a thermometer and a barometer, respectively.

The test procedure was repeated five times, so for each of the radial positions there were five determinations of the experimental velocity  $v$ . These were averaged to give a mean result at each position and used for obtaining the graphs shown in Figure 3 and Figure 4. A maximum standard deviation of 0.5 m/s was detected, corresponding to a random uncertainty of 1 m/s.

Velocity measurements were repeated over axial sections of the jet at a distance  $x$  from the nozzle exit equal to 74 and 90 mm.

The performances of the nozzles were compared, imposing a constant air consumption equal to an acceptable value (55 dm<sup>3</sup>/min (ANR)). Consequently, tests were carried out setting each nozzle supply pressure at a value corresponding to the desired flow rate. In the case of nozzle A and nozzle D, the supply gauge pressure was set at 2,8 bar, because their pneumatic conductances were the same (see Table 2). The supply gauge pressure of nozzle B was set at 3,4 bar.

As an example of the results obtained, Figure 3 shows the jet velocity profiles obtained for nozzle A, nozzle B and nozzle D, respectively; in particular, jet axial sections at a distance of 40 mm and 90 mm from the nozzle exit can be compared.

As shown, in all cases, the longer is distance  $x$ , the larger and the slower is the jet. The jet enlargement is due to the viscous interaction between its high velocity particles and the surrounding particles, which are initially at rest; ambient particles are accelerated by the jet and sucked inside it. At the same time, the boundary layer around the jet is progressively slowed down, until the jet is completely dispersed.

As shown, the jet from the porous nozzle (nozzle A) was found to be slower than the one from nozzle D, with a greater spread; on the basis of previous observations, this can be justified

considering it has a larger surface interacting with the surroundings. As a consequence, a lower efficiency in terms of yarn dragging can be expected.

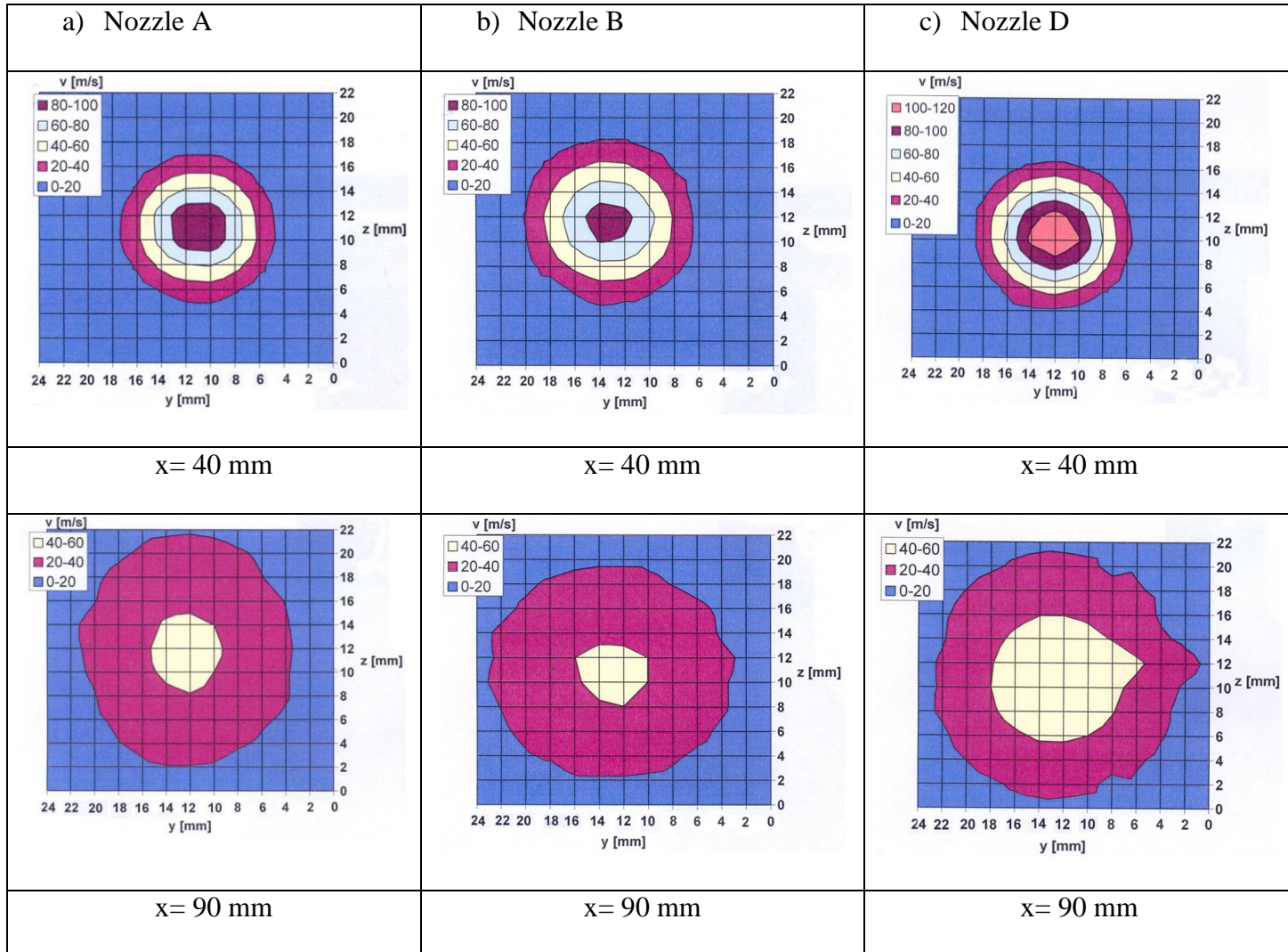


Figure 3 Jet velocity profiles at distance  $x = 40$  mm and  $x = 90$  mm from the nozzle emitting cross-section: a) nozzle A; b) nozzle B; c) nozzle D.

Comparing the two single hole nozzles (nozzle B and nozzle D), the better performance of nozzle D is due to its higher conductance.

It must be remarked that the velocity profiles were all drawn centering them on a 24 mm x 22 mm layer, in order to allow a quick comparison of their shape and spreading. Actually, the  $z$ -coordinate of the jet's center increases with  $x$  position because of the inclination of the jet with respect to the



horizontal direction; in particular, jet angles of  $8^\circ$ ,  $13^\circ$  and  $12^\circ$  were found for nozzle A, nozzle B and nozzle D respectively.

Figure 4 summarises all results obtained, showing jets maximum velocity, that is, the jet's axial velocity, at various distances from the nozzle's emitting cross-section. As shown, the maximum jet velocity values change with the nozzles, but the trend is in all cases is similar to that of a nozzle with a single axisymmetric hole. The jet from nozzle D exhibited the highest axial velocity over the overall distance considered from the nozzle exit.

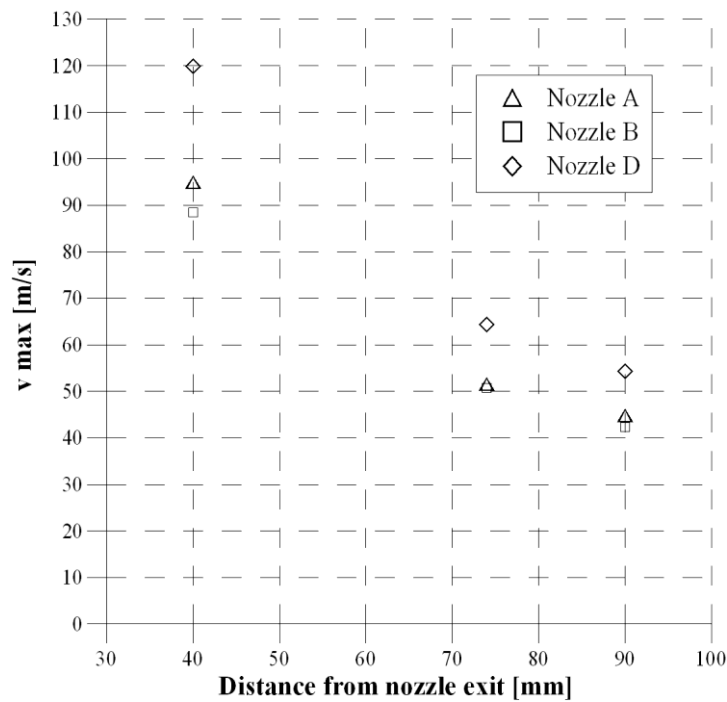


Figure 4 Jet's axial velocity at various distance from the nozzle exit.

### 3. Drag force measurement

Since the ability to drag the weft yarn along the profiled reed is the main requirement of a sub-nozzle, tests aimed at measuring the drag force exerted by the sub-nozzles airflow on a piece of yarn were carried out. As shown in Figure 5, the tail of a 300 mm long piece of yarn was fixed to a load cell (full scale = 0.5 N; accuracy = 0.1%), while its tip was left free. The distance between the sub-nozzle and the yarn free tip was put equal to 74 mm, because this was the mounting distance between two sub-nozzles on the loom.

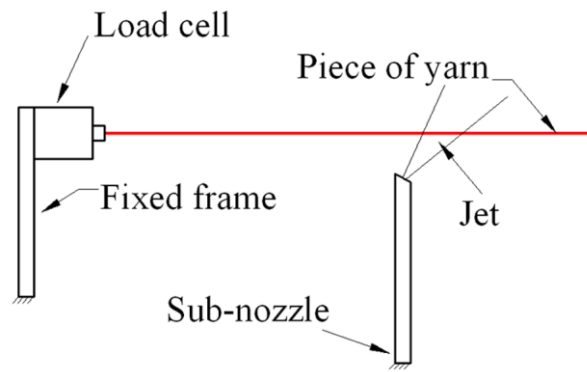


Figure 5 Experimental set-up for drag force measurement.

Since the force required to move the yarn mass is provided exclusively by air friction against the yarn structure, it is largely dependent on the yarn structure, the yarn and fibre surface and the relative motion of air and yarn. In particular, monofilament yarns are difficult to weave by an air-jet loom because of their smooth surface and consequent low friction between air and yarn [7]. In order to analyse the worst case, a monofilament nylon yarn ( diameter = 0.08 mm) was used during tests. When supply air was provided to the tested sub-nozzle, strai was put on the yarn by the airflow. The load cell measured the mean drag force exerted by the air jet on the intercepted piece of yarn; a flow-meter measured the nozzle consumption. Tests were carried out regulating the nozzles supply pressure so that their consumption varied from 15 to 95 dm<sup>3</sup>/min ANR. The test procedure was repeated three times, so for each nozzle consumption there were three determinations of the experimental drag force. These were averaged to give a mean result, as shown on Figure 6.

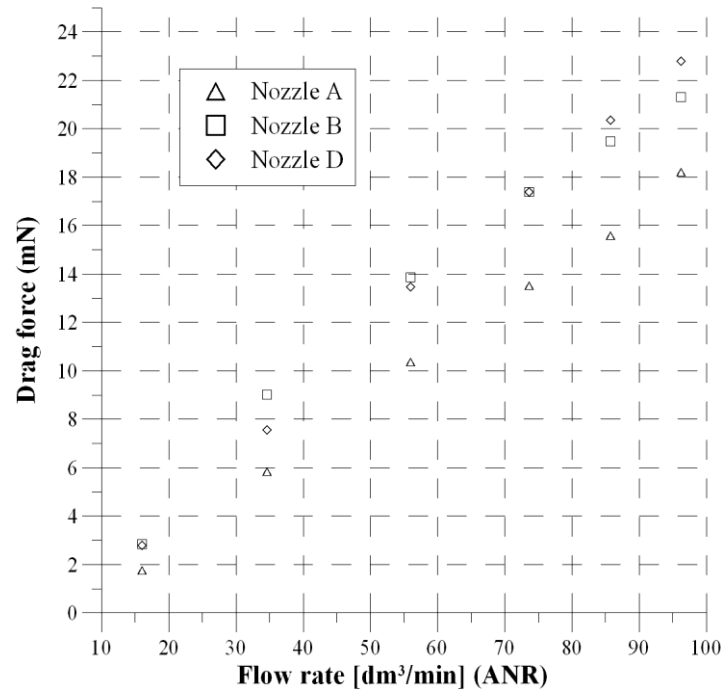


Figure 6 Drag force on a piece of yarn, varying sub-nozzles' consumption.

The results obtained confirmed what could be inferred from the analysis of the jet velocity profiles. In fact, drag force is due to the shear stresses, that is, the friction exerted by the airflow on the yarn surface. Shear stresses largely depend on the air velocity gradient; the higher is the jet velocity, the higher is the shear stress and, consequently, the higher is the drag force.

Nozzle A was found to be less effective in dragging the yarn because, even if its jet had the same velocity of that of nozzle B, it had a smaller inclination angle with respect to the horizontal direction; consequently it interacted with the yarn at a lower velocity than the single-hole nozzles. Conversely, comparing the two single-hole nozzles, the jet from nozzle B was slower than that from nozzle D but it had a larger angle of inclination. These characteristics caused nozzle B and nozzle D to have almost the same performance.

#### 4. Velocity distribution inside the weft passage

The jet emitted by a sub-nozzle in an air-jet loom cannot be considered to be a free jet, because of the interaction with the profiled reed. In order to analyse the airflow through the weft passage,

which the weft yarn motion depends on, some measurements were repeated, mounting the sub-nozzle on an air-jet loom as in actual operating conditions. Figure 7 shows the sub-nozzle positioning with respect to the profiled reed.

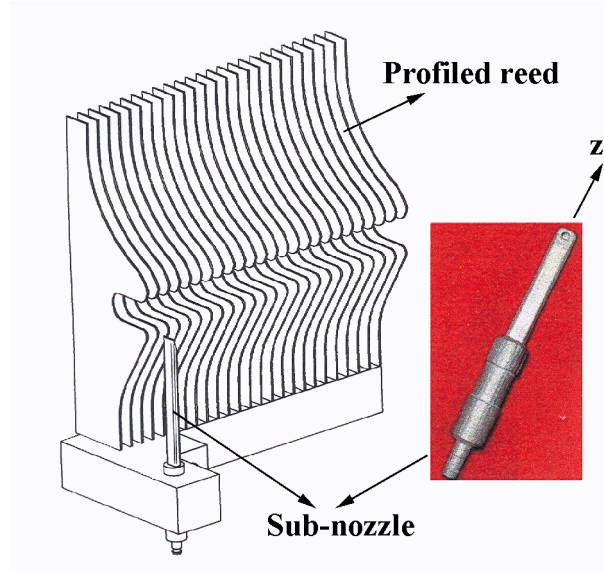


Figure 7 Sub-nozzle positioning with respect to the profiled reed.

Using the test arrangement shown in Figure 5, where the fixed frame was the loom, preliminary tests were carried out to identify the most effective orientation of each sub-nozzle with respect to its z-axis. The final orientation of each sub-nozzle corresponded to the configuration that gave the maximum drag force, with an air consumption of  $55 \text{ dm}^3/\text{min}$  (ANR).

Subsequently, velocity measurements were carried out inside the profiled reed by means of a Pitot probe. Tests were carried out using the same equipment and following the same procedure described for obtaining free jets velocity profiles. Having placed the Pitot probe at a fixed distance from the nozzle exit, it was displaced inside the profile reed using the precision manual positioner, with a step of 1 mm along the y-axis and the z-axis. Tests were carried out at various distances from the nozzle exit ( $x = 40, 60, 74 \text{ mm}$ ).

As an example of results, Figure 8 shows the velocity field inside the profiled reed due to nozzle B, at a distance  $x = 40 \text{ mm}$  from the nozzle exit. As shown, the maximum velocity values were

reached inside the concave profile of the loom reed, at the upper side. This behaviour was exhibited by all nozzles tested, except for the porous one (nozzle A). In this case, a more uniform velocity field was obtained inside the weft passage, but lower velocity values were reached.

Figure 8 Velocity values [m/s] inside the weft passage at 40 mm from nozzle B exit.

Finally, a high-speed camera (8000 frames/s) was used to visualize the behaviour of a weft yarn flying across the profiled reed. Figure 9 a) shows the weft yarn tip crossing before the sub-nozzle; then, the weft yarn tip is pushed by the sub-nozzle airflow and is placed within the high velocity area (Figure 9 b)); it can be supposed that the weft yarn tip corresponds to the free jet axis.

Conversely, the rest of the yarn tended to fly near the reed tunnel bottom (Figure 9 c)).

These observations confirmed the importance of the relationship between velocity profiles and drag effect; it was also confirmed that limiting the sub-nozzles operation time is a proper choice, since the effectiveness of the sub-nozzles airflow is limited to the first part of the weft yarn intercepted by the sub-nozzle airflow. Between one sub-nozzle and the next one, the yarn slides almost without friction over the reed tunnel bottom. The system limitations were also pointed out: because of the geometry, the weft yarn is forced against the reed teeth, inside the high velocity zone and could come into contact with the reed teeth, with sliding friction.

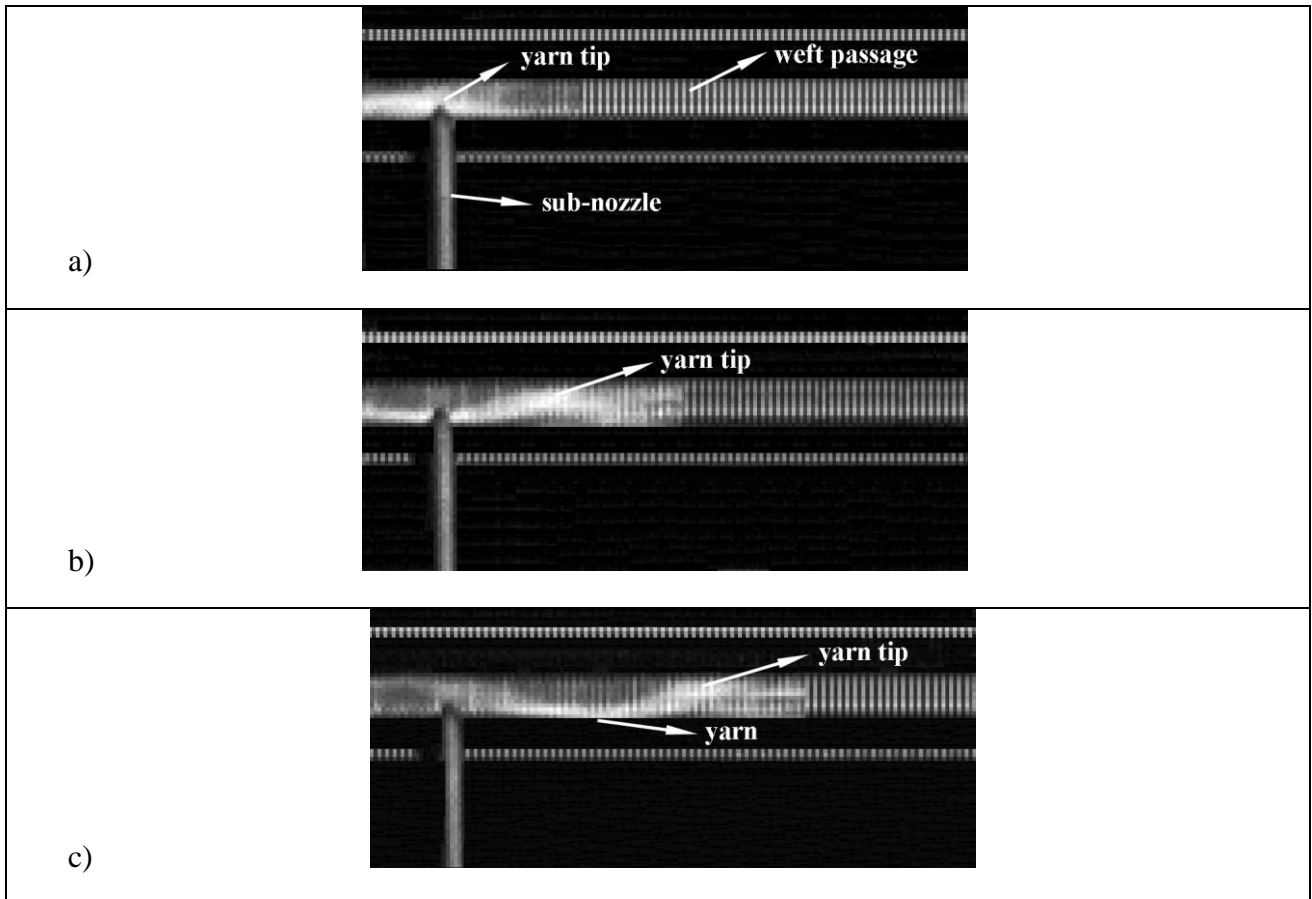


Figure 9 Observation of the yarn crossing the weft passage.

## Conclusions

Sub-nozzles having different geometry were analysed and their performance were compared taking constant air consumption. It was found that, already at short distances from the nozzle exit, the jet shape is always similar to that obtained with a single axisymmetric hole nozzle.

Drag force measurements, which gave a simple and effective way to optimise the sub-nozzles positioning on the loom, confirmed that the best performances could be obtained by using single hole nozzles. In fact, the jet emitted by the porous nozzle was found to slow down more quickly by interaction with the surroundings, because of its larger interacting surface. Consequently, the use of this kind of nozzle could only be justified by reasons other than those analysed here.

The influence of the nozzle feeding duct on its performance was highlighted. The nozzle overall conductance, in fact, is determined by the series of a conductance associated to its feeding duct and of a conductance associated to its emitting cross-section. A feeding duct designed so to reduce pressure drops and to guide the flow as much as possible towards the exit section can increase the nozzle pneumatic conductance; therefore, the same performance can be obtained by using a lower supply pressure, in other words saving energy.

Velocity measurements inside the weft passage highlighted that the maximum velocity values were reached inside the concave profile of the loom reed, on the upper side. Observations by a high-speed camera highlighted that only the yarn tip is located within the high velocity area, while the rest of the yarn tended to fly near the reed tunnel bottom.

## References

- [1] L. Vangheluwe, “Air-jet weft insertion – Textile progress”, Vol. 29, No. 4, Woodhead publishing (1999).
- [2] M. Ishida, A. Okajima, “Flow characteristics of main nozzle in an air-jet loom”, *Textile Research Journal*, **64**, pp.10-20 (1994).
- [3] O. Göktepe, O. Bozkan, “Study on reduction of air consumption on air-jet weaving machines”, *Textile Research Journal*, **78** (9), pp.816-824 (2008).
- [4] R. Shintani, A. Okajima, “Air flow through a weft passage of profile reed in air jet looms”, *Journal of the Textile Machinery Society of Japan*, **54**, pp.56-63 (2001).

- [5] G.Belforte, A.Costamagna, G.Mattiazzi, F.Testore, C. Visconte, “Flow field characterization of air-jet loom auxiliary nozzles”, AUTEX 2008 – World Textile Conference, Biella, (2008).
- [6] ISO 6358 “Pneumatic fluid power -Components using compressible fluids -Determination of flow-rate characteristics”, (1989).
- [7] Adanur S., “Handbook of weaving”, CRC Press, (2000).